Commensurate-incommensurate solid transition in the ^{4}He monolayer on γ-graphyne

Jeonghwan Ahn, Hoonkyung Lee, and Yongkyung Kwon*

Division of Quantum Phases and Devices, School of Physics, Konkuk University, Seoul 143-701, Korea

(Received 27 May 2014; revised manuscript received 14 August 2014; published 27 August 2014)

Path-integral Monte Carlo calculations have been performed to study the ^{4}He adsorption on γ-graphyne, a planar network of benzene rings connected by acetylene bonds. Assuming the ^{4}He-substrate interaction described by a pairwise sum of empirical ^{4}He-carbon interatomic potentials, we find that unlike α-graphyne, a single sheet of γ-graphyne is not permeable to ^{4}He atoms in spite of its large surface area. One-dimensional density distributions computed as a function of the distance from the graphyne surface reveal a layer-by-layer growth of ^{4}He atoms. A partially-filled ^{4}He monolayer is found to exhibit different commensurate solid structures depending on the helium coverage; it shows a $C_{2/3}$ commensurate structure at an areal density of 0.0491 Å^{-2}, a $C_{3/3}$ structure at 0.0736 Å^{-2}, and a $C_{4/3}$ structure at 0.0982 Å^{-2}. While the promotion to the second layer starts beyond the $C_{4/3}$ helium coverage, the first ^{4}He layer is found to form an incommensurate triangular solid when compressed with the development of the second layer.

DOI: 10.1103/PhysRevB.90.075433 PACS number(s): 67.25.bd, 67.25.bh, 67.80.B−, 75.10.−b

For the past few decades, a system of ^{4}He atoms adsorbed on a substrate has been intensively studied to investigate physical properties of low-dimensional quantum fluids. Carbon allotropes have often been chosen as substrates for this purpose because they provide strong enough interactions for ^{4}He adsorbates to show multiple distinct layered structures [1]. As a result of the interplay between ^{4}He-^{4}He and ^{4}He-substrate interaction, these helium adlayers are known to exhibit rich phase diagrams including various commensurate and incommensurate solids. On the surface of graphite, a monolayer of ^{4}He atoms was observed to be crystallized to a $C_{1/3}$ commensurate solid at an areal density of 0.0636 Å^{-2} and to go through various domain structures before freezing into an incommensurate triangular solid as the helium coverage increases [2,3]. Similar quantum phase transitions were predicted for the ^{4}He monolayer on a single graphene sheet [4–6]. While no superfluidity has been observed in the first ^{4}He layer, the second layer on graphite does show finite superfluid response at intermediate helium coverages as first revealed by torsional oscillator measurements of Crowell and Reppy [3]. These experimentally-identified quantum phases of the ^{4}He layers on graphite were confirmed by path-integral Monte Carlo (PIMC) calculations performed first by Pierce and Manousakis [7–11] and later by Corboz *et al.* [12]. Whether the second-layer superfluid phenomenon is related to two-dimensional supersolidity, however, is still an ongoing issue pursued heavily by some experimentalists.

The ^{4}He adsorption on the surface of a carbon allotrope other than graphite or graphene has recently been investigated. While ^{4}He atoms adsorbed on the interstitials or the groves of carbon nanotube bundles showed characteristics of one-dimensional quantum fluid [13,14], a series of theoretical calculations predicted well-distinct layered structures for ^{4}He atoms adsorbed on the outer surfaces of fullerene molecules with each near-spherical helium layer exhibiting various quantum states depending on the number of ^{4}He adatoms [15–18]. More recently, graphynes, $sp-sp^2$ hybridized two-dimensional networks of carbon atoms [19–21], have attracted much interest because of their intriguing electronic features such as both symmetric and asymmetric Dirac cones [22,23] and high carrier mobility [24]. Furthermore, they have much larger surface area than graphene, which has prompted intensive investigation of their possible applications as high-capacity hydrogen storage [25,26] and Li-ion battery anode materials [27]. Using the PIMC method, two of us recently studied the ^{4}He adsorption on α-graphyne [28], a honeycomb structure of both sp^2-bonded carbon atoms and sp-bonded ones. Due to the presence of much larger hexagons than those of graphene, in-plane adsorption of ^{4}He atoms was observed on α-graphyne with a single ^{4}He atom being embedded to the center of each hexagon. The first layer of ^{4}He atoms adsorbed on the ^{4}He-embedded α-graphyne was found to undergo a Mott-insulator to commensurate-solid transition which was interpreted as a transition from a spin liquid of frustrated antiferromagnets to a ferromagnetic phase with the introduction of Ising pseudospins based on the sublattice symmetry of the honeycomb structure [28].

Here we have performed the PIMC simulations to study the ^{4}He adsorption on γ-graphyne, the most stable structure among graphynes [29]. With the increasing number of ^{4}He adatoms, multiple distinct helium layers are observed on γ-graphyne. Because of larger hexagons of graphyne, these ^{4}He adsorbates show a richer phase diagram than the corresponding ones on graphite or graphene. Unlike α-graphyne, however, even a single sheet of γ-graphyne is found to be impermeable to ^{4}He atoms. It is found that the ^{4}He monolayer exhibits various commensurate solid structures at different areal densities before crystallizing into an incommensurate triangular solid at its completion.

In this study, a single γ-graphyne sheet is fixed at $z = 0$ and the helium-graphyne interaction is described by a sum of pair potentials between the carbon atoms and a ^{4}He atom. For the ^{4}He-C interatomic potential, we use an isotropic 6-12 Lennard-Jones potential proposed by Carlos and Cole [30] to fit helium scattering data from graphite surfaces. While Fig. 1(a) shows a contour plot of the minimum potential energy $V_{\min}(x,y)$ above each point (x,y) on the graphyne surface,

*ykwon@konkuk.ac.kr

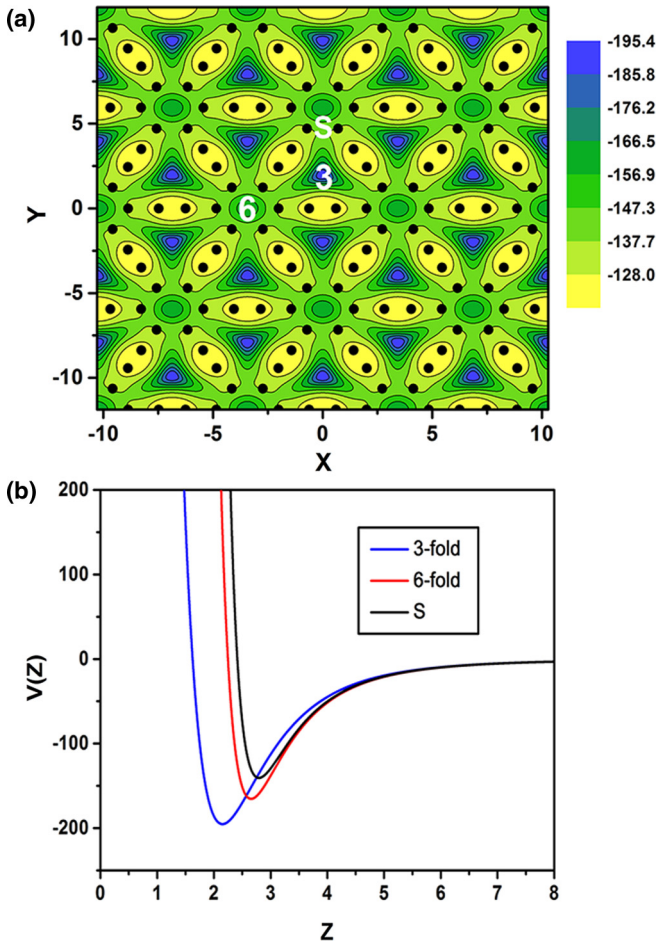

FIG. 1. (Color online) (a) A contour plot of the minimum ^{4}He-graphyne potential, $V_{\min}(x,y)$, above each point (x,y) on γ-graphyne and (b) the ^{4}He-graphyne potential as a function of the distance z from the graphyne surface along different symmetry directions. The black dots in (a) represent the positions of carbon atoms on the γ-graphyne surface. In (b), the blue, the red, and the black line correspond to the threefold symmetry direction, the sixfold direction, and the direction of a saddle point [see white numbers and letter S in (a)], respectively. The length unit is Å and the potential energies are in units of Kelvin.

Fig. 1(b) presents our ^{4}He-graphyne potential as a function of the distance z from graphyne along three different symmetry directions perpendicular to the graphyne surface. As seen in Fig. 1(a), there are three adsorption sites per graphyne unit cell: two global minima of the ^{4}He-graphyne potential located at the centers of big irregular hexagons and one local minimum located at the center of a small regular hexagon (or a benzene ring). A bigger hexagon, which has much larger area than a smaller one, is expected to accommodate more than one ^{4}He atom. Figure 1(b) shows that the global minima in the threefold symmetry directions are located closer to the graphyne surface by $\sim$0.5 Å than the local minima in the sixfold symmetry directions, and the potential energy difference between them is as large as $\sim$30 K. From this we conjecture that the ^{4}He adatoms predominantly occupy the global minimum sites at low helium coverages, rather than the local minima. We here note that there is a strong repulsive potential barrier for ^{4}He atoms as they approach the graphyne surface, i.e., $z \to 0$, suggesting that ^{4}He atoms cannot penetrate through a γ-graphyne sheet from one side to the other.

We here note that this approach of modeling ^{4}He-substrate potential with a pairwise sum of the empirical ^{4}He-C interatomic potentials has some limitation in describing the ^{4}He-graphyne interaction because graphyne involves sp-bonded C atoms as well as sp^2-bonded ones. Without a more plausible ^{4}He-graphyne potential, we tested the reliability of our PIMC results by varying the well depth of the ^{4}He-C pair potential; little change was observed in the structural features of the ^{4}He adlayers when the potential well between ^{4}He and sp carbon varied by $\pm 15\%$ from the ^{4}He-C potential well for sp^2 carbon. From this we expect that the main PIMC results presented here will be preserved when more accurate ^{4}He-graphyne potential is available. For the ^{4}He-^{4}He interaction, we use a well-known Aziz potential [31]. Since the exact form of thermal many-body density matrix is not known at a low temperature T, one can resort to the path-integral representation where the low-temperature density matrix is expressed by a convolution of M high-temperature density matrices with an imaginary time step $\tau = 1/(Mk_BT)$. Both ^{4}He-^{4}He and ^{4}He-C pair potentials are used to derive the exact two-body density matrices at the high temperature MT [32,33], which was found to provide an accurate description of the ^{4}He-graphyne interaction as well as the ^{4}He-^{4}He interaction with an imaginary time step of $(\tau k_B)^{-1} = 40$ K. We employ the multilevel Metropolis algorithm described in Ref. [32] to sample the imaginary time paths as well as the permutations among ^{4}He atoms. To minimize finite size effects, periodic boundary conditions are applied to a fixed 3×2 rectangular simulation cell with dimensions of 20.58×23.76 Å^2. All PIMC simulations presented here started from random initial configurations of ^{4}He atoms.

Here we consider the ^{4}He adsorption only on one side of the graphyne sheet, i.e., $z > 0$. Figure 2 presents one-dimensional ^{4}He density distributions as a function of distance z from the

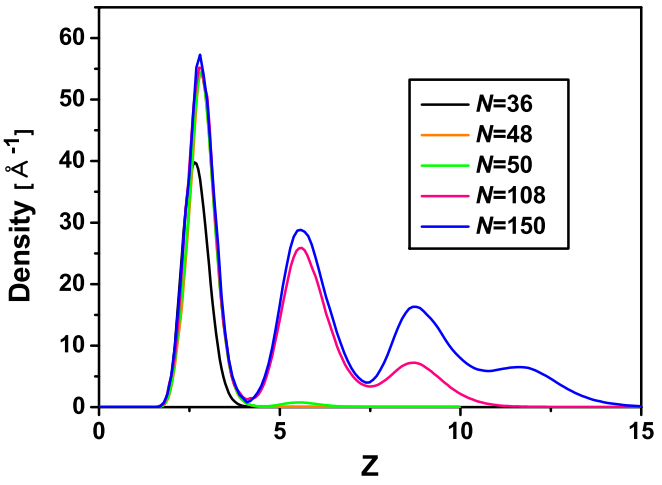

FIG. 2. (Color online) One-dimensional density of ^{4}He atoms adsorbed on a single γ-graphyne sheet as a function of the distance z (in Å) from the graphyne surface. Here N represents the number of ^{4}He adatoms per 3×2 rectangular simulation cell with dimensions of 20.58×23.76 Å^2, and the computations were done at a temperature of 0.5 K.

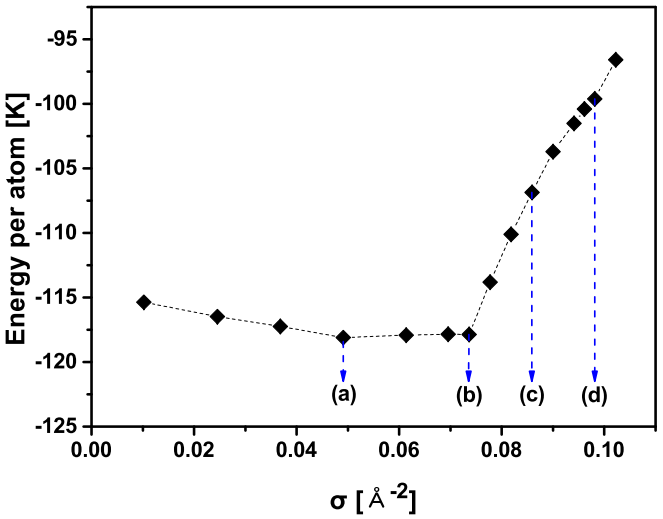

FIG. 3. (Color online) Energy per ^{4}He atom of the first ^{4}He layer on γ-graphyne as a function of the helium coverage. The letters (a), (b), (c), and (d) correspond to the areal densities of 0.0491, 0.0736, 0.0859, and 0.0982 Å^{-2}, respectively, for which two-dimensional ^{4}He density plots are shown in Fig. 4. The energies were computed at a temperature of 0.5 K.

graphyne surface for different numbers of ^{4}He adatoms N per 3×2 rectangular simulation cell. These density distributions confirm the above assertion that ^{4}He atoms cannot penetrate to the other side of $z < 0$ through a single graphyne sheet because of the presence of the strong repulsive potential barrier. As more ^{4}He atoms are adsorbed, one can see the development of layered structures as evidenced by well-distinct density peaks in Fig. 2. The first sharp peak is located at $z \sim 2.7$ Å and the second peak at $z \sim 5.8$ Å, similar to the case of ^{4}He on graphene [5]. We observe the emergence of the ^{4}He second layer when the number of ^{4}He adatoms per 3×2 simulation cell increases beyond $N = 48$ (an areal density of 0.0982 Å^{-2}). With further development of the second helium layer, more ^{4}He atoms are found to be squeezed into the first layer. From this we conjecture that the completed first layer would be a compressible incommensurate solid like the corresponding layer on graphene [5] or graphite [2,12]. It is found that the first layer is completed at an areal density of $\sim$0.115 Å^{-2} while the corresponding value on graphene was predicted to be $\sim$0.12 Å^{-2} [5]. This small (about 4%) difference suggests that the ^{4}He-graphene potential is more attractive than the ^{4}He-graphyne potential and graphene may accommodate more ^{4}He atoms in its immediate vicinity than graphyne.

Now we discuss the energetics of the ^{4}He-graphyne system, which provides some insight into the growth of the ^{4}He adlayers on γ-graphyne and their different quantum phases. Figure 3 shows the energy per ^{4}He atom as a function of an areal density σ. Since the energies presented here were computed at a low temperature of 0.5 K, they are close to the ground-state energies, the zero-temperature free energies, allowing us to use them to conjecture different quantum phases depending on the helium coverage. At low densities of $\sigma < 0.0736$ Å^{-2}, the energy per ^{4}He atom changes very little, indicating that each ^{4}He atom occupies one of the adsorption sites, i.e., the ^{4}He-graphyne potential minima. It is found that the energy per atom has the lowest value at $\sigma = 0.0491$ Å^{-2} which corresponds to two ^{4}He atoms per the graphyne unit cell. Noting that there are two global minima of the ^{4}He-graphyne potential per the unit cell [see Fig. 1(a)], we conjecture that in the lowest energy state at $\sigma = 0.0491$ Å^{-2} each global minimum site is occupied by a single ^{4}He atom. After filling all global minima, additional ^{4}He atoms are expected to occupy the local minima located above the centers of the small hexagons, which is consistent with a slight increase in the energy per atom for 0.0491 Å$^{-2} < \sigma < 0.0736$ Å^{-2}. Since the distances between the adsorption sites on the graphyne surface are long enough ($\sim$4 Å), the ^{4}He-^{4}He interaction is understood to have minimal effects while ^{4}He atoms are filling these adsorption sites. Each adsorption site, whether it is a global minimum or a local minimum, is occupied by a single ^{4}He atom at an areal density of $\sigma = 0.0736$ Å^{-2}, three ^{4}He atoms per the graphyne unit cell, beyond which one can observe a sudden increase in the energy per atom in Fig. 3. The continuous increase of the energy per atom for $\sigma > 0.0736$ Å^{-2} suggests that the ^{4}He-^{4}He interaction as well as the ^{4}He-substrate interaction plays a critical role in determining quantum states of the ^{4}He monolayer at high helium coverages. One can observe a significant jump in the energy per atom at an areal density of $\sigma = 0.0982$ Å^{-2}, which reflects the start of the second-layer promotion concluded in the analysis of the one-dimensional density distributions of Fig. 2.

For further analysis of different phases of the ^{4}He monolayer, we computed two-dimensional density distributions of ^{4}He adatoms on γ-graphyne at various areal densities. In all four density plots presented in Fig. 4, a distinct density peak represents the occupancy of a single first-layer ^{4}He atom. At an areal density of 0.0491 Å^{-2}, which corresponds to the lowest energy state, each of the irregular hexagons is seen in Fig. 4(a) to accommodate one ^{4}He atom at its center, confirming our conjecture made from the energetic analysis. These ^{4}He atoms form a honeycomb structure with the same primitive vectors as those of the underlying graphyne triangular lattice, which is therefore a 1×1 registered phase in the Wood's notation. It is also a $C_{2/3}$ commensurate solid with two out of every three adsorption sites being occupied by ^{4}He atoms. The lowest-energy state for the ^{4}He monolayer on graphene is a $C_{1/3}$ commensurate solid [4]. We note that the $C_{2/3}$ commensurate solid on graphyne is realized at an areal density significantly lower than the $C_{1/3}$ commensurate helium coverage of 0.0636 Å^{-2} on graphene. Furthermore, vacancies created in this $C_{2/3}$ solid on graphyne are found to be immobile and very weakly, if ever, interacting with each other, which could be understood by high potential barrier and long distances between the neighboring adsorption sites.

As conjectured above, the local minima located at the centers of the small regular hexagons accommodate additional ^{4}He atoms beyond the $C_{2/3}$ commensurate coverage. Figure 4(b) shows another commensurate structure at an areal density of $\sigma = 0.0736$ Å^{-2}, where each of the adsorption sites, both global minima and local minima, is occupied by a single ^{4}He atom. In this $C_{3/3}$ commensurate structure,

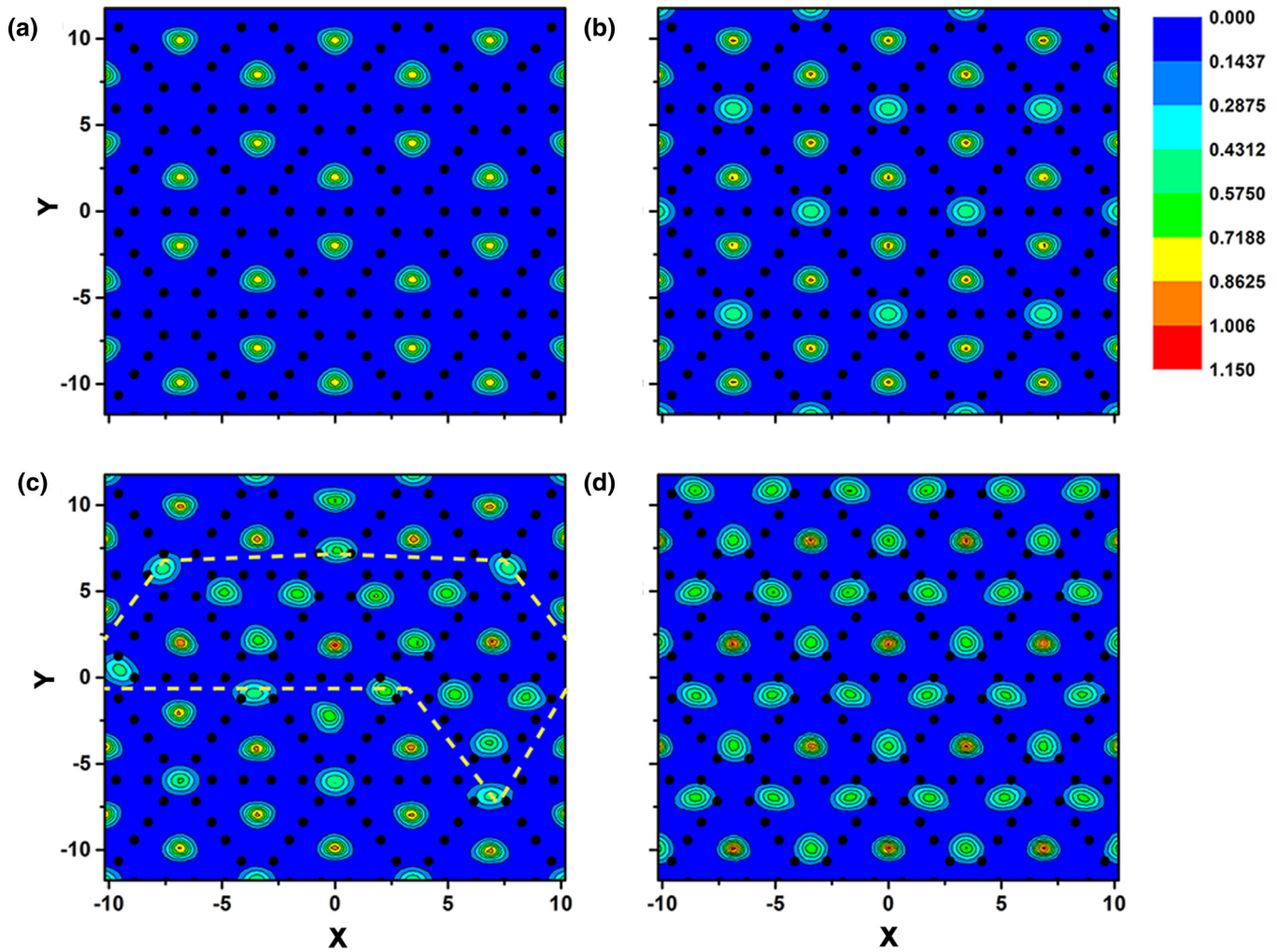

FIG. 4. (Color online) Two-dimensional density distributions of the first-layer ^{4}He atoms adsorbed on a single γ-graphyne sheet at areal densities of (a) 0.0491, (b) 0.0736, (c) 0.0859, and (d) 0.0982 Å^{-2}. The black dots represent the positions of the carbon atoms of graphyne. The length unit is Å and all contour plots are in the same color scale denoted by the color table in the upper right hand corner. The yellow dotted lines in (c) separate two different domains from each other. The PIMC calculations were done at a temperature of 0.5 K.

the ^{4}He adatoms form a triangular solid structure registered by $\frac{1}{\sqrt{3}} \times \frac{1}{\sqrt{3}}$ to the graphyne triangular lattice. With further increase of the helium coverage beyond the $C_{3/3}$ solid, where the energy per ^{4}He atom increases monotonically as shown in Fig. 3, the ^{4}He monolayer enters a regime of various domain structures. At higher ^{4}He coverages, the ^{4}He-^{4}He interaction as well as the ^{4}He-substrate interaction is expected to affect the structure of the ^{4}He monolayer. At an areal density of 0.0859 Å^{-2}, one can observe two different domains separated by the yellow dotted lines in Fig. 4(c); one domain involves some irregular hexagons accommodating three ^{4}He atoms while the other consists of the ^{4}He atoms in the $C_{3/3}$ commensurate order. Another homogeneous phase of the ^{4}He monolayer is observed at an areal density of 0.0982 Å^{-2}, where all ^{4}He atoms are accommodated by irregular hexagons and no small hexagon includes a ^{4}He atom. In this phase, some irregular hexagons accommodate three ^{4}He atoms and the neighboring ones include only one ^{4}He atom. With an alternating order of the three-atom and the single-atom irregular hexagons, the ^{4}He atoms constitute another perfect triangular solid whose primitive vectors are one half of those of the underlying graphyne structure. This $\frac{1}{2} \times \frac{1}{2}$ registered phase is a $C_{4/3}$ commensurate solid with 4 ^{4}He atoms being accommodated by a graphyne unit cell. We note that Li atoms attached to γ-graphyne could constitute an in-plane structure similar to this $C_{4/3}$ solid as reported in Ref. [27]. As discussed above, additional ^{4}He atoms beyond the $C_{4/3}$ commensurate coverage of 0.0982 Å^{-2} are promoted to the second layer that is a fluid at a low areal density like the corresponding layer on graphite. With further development of the second ^{4}He layer, more ^{4}He atoms are found to be squeezed into the first layer. The fully-compressed first layer shows an incommensurate triangular lattice structure like the corresponding layer on graphite.

The structural features of the helium monolayer on γ-graphyne described above were also observed in the PIMC calculations for a larger system. Figure 5 shows the peak values of the static structure factors divided by the number

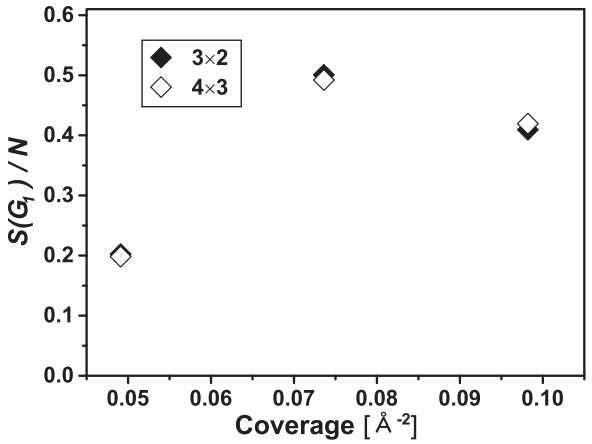

FIG. 5. The peak values of the static structure factor divided by the number of ^{4}He atoms in the first helium layer on γ-graphyne, at three different commensurate helium coverages. Here G_1 represents the primitive vector of the reciprocal lattice of the corresponding commensurate solid. The solid (open) diamonds represent the PIMC data for the 3×2 (4×3) rectangular simulation cell, and the statistical errors are smaller than the symbol sizes.

of ^{4}He adatoms at three different commensurate helium coverages, which were computed for both 3×2 and 4×3 simulation cells. For all helium coverages considered here the structure factors are found to be peaked at the reciprocal primitive vectors of the corresponding commensurate solids, whose magnitudes are 1.0576 Å^{-1} at an areal density of $\sigma =$ 0.0491 Å^{-2} ($C_{2/3}$ solid), 1.8318 Å^{-1} at $\sigma = 0.0736$ Å^{-2} ($C_{3/3}$ solid), and 2.1152 Å^{-1} at $\sigma = 0.0982$ Å^{-2} ($C_{4/3}$ solid). Little difference between the results for the two different system sizes suggests that the main structural features, especially three different commensurate solid structures, are not affected by the finite sizes of our systems while the shapes of the domain walls as shown in Fig. 4(c) might depend on the geometry of the simulation cell.

Our PIMC calculations have shown multiple distinct ^{4}He layers on a single sheet of γ-graphyne which is not permeable to ^{4}He atoms unlike α-graphyne. As in the case of ^{4}He on graphite, the first ^{4}He layer on γ-graphyne exhibits a commensurate-incommensurate solid transition after going through some domain-wall phases. It is compressed by the development of the second layer to become an incommensurate triangular solid when filled completely. However, the ^{4}He monolayer on graphyne can be crystallized into three different commensurate solid structures at different partial helium coverages such as a 1×1, a $\frac{1}{\sqrt{3}} \times \frac{1}{\sqrt{3}}$, and a $\frac{1}{2} \times \frac{1}{2}$ registered phase, while the corresponding helium layer on graphite shows only one commensurate structure of a $\sqrt{3} \times \sqrt{3}$ phase. A richer phase diagram shown by the ^{4}He layer on graphyne can be attributed to the fact that graphyne is more porous than graphite, and a larger hexagonal cell of graphyne can accommodate more than one ^{4}He atom (see Fig. 1). While some theoretical calculations predicted that zero-point vacancies would not be thermodynamically stable in bulk solid ^{4}He [34–36], a substrate potential could stabilize the vacancy formation in a commensurate ^{4}He solid on a substrate. Therefore the existence of a stable commensurate structure is understood to be critical in realizing the vacancy-based supersolidity proposed originally by Andreev and Lifshitz [37]. Unlike the $C_{1/3}$ commensurate solid of ^{4}He atoms on graphite where no superfluidity was observed [9], one of the three commensurate structures found in the ^{4}He monolayer on γ-graphyne could manifest the superfluid response induced by vacancies, which is now under our investigation.

This work was supported by the Basic Science Research Program (2012R1A1A2006887) through the National Research Foundation of Korea funded by the Ministry of Education, Science and Technology. We also acknowledge the support from the Supercomputing Center/Korea Institute of Science and Technology Information with supercomputing resources including technical support (KSC-2014-C3-001).

[1] G. Zimmerli, G. Mistura, and M. H. W. Chan, Phys. Rev. Lett. **68**, 60 (1992).
[2] D. S. Greywall, Phys. Rev. B **47**, 309 (1993).
[3] P. A. Crowell and J. D. Reppy, Phys. Rev. B **53**, 2701 (1996).
[4] M. C. Gordillo and J. Boronat, Phys. Rev. Lett. **102**, 085303 (2009).
[5] Y. Kwon and D. M. Ceperley, Phys. Rev. B **85**, 224501 (2012).
[6] J. Happacher, P. Corboz, M. Boninsegni, and L. Pollet, Phys. Rev. B **87**, 094514 (2013).
[7] M. Pierce and E. Manousakis, Phys. Rev. Lett. **81**, 156 (1998).
[8] M. Pierce and E. Manousakis, Phys. Rev. B **59**, 3802 (1999).
[9] M. E. Pierce and E. Manousakis, Phys. Rev. Lett. **83**, 5314 (1999).
[10] M. E. Pierce and E. Manousakis, Phys. Rev. B **62**, 5228 (2000).
[11] D. M. Ceperley and E. Manousakis, J. Chem. Phys. **115**, 10111 (2001).
[12] P. Corboz, M. Boninsegni, L. Pollet, and M. Troyer, Phys. Rev. B **78**, 245414 (2008).
[13] M. W. Cole, V. H. Crespi, G. Stan, C. Ebner, J. M. Hartman, S. Moroni, and M. Boninsegni, Phys. Rev. Lett. **84**, 3883 (2000).
[14] M. C. Gordillo, Phys. Rev. Lett. **101**, 046102 (2008).
[15] Y. Kwon and H. Shin, Phys. Rev. B **82**, 172506 (2010).
[16] H. Shin and Y. Kwon, J. Chem. Phys. **136**, 064514 (2012).
[17] H. Shin and Y. Kwon, J. Chem. Phys. **138**, 064307 (2013).
[18] S. Park and Y. Kwon, Phys. Rev. E. **89**, 042118 (2014).
[19] R. H. Baughman, H. Eckhardt, and M. Kertesz, J. Chem. Phys. **87**, 6687 (1987).
[20] V. R. Coluci, S. F. Braga, S. B. Legoas, D. S. Galvão, and R. H. Baughman, Phys. Rev. B **68**, 035430 (2003).
[21] V. R. Coluci, S. F. Braga, S. B. Legoas, D. S. Galvão, and R. H. Baughman, Nanotechnology **15**, S142 (2004).
[22] D. Malko, C. Neiss, F. Viñes, and A. Görling, Phys. Rev. Lett. **108**, 086804 (2012).

[23] B. G. Kim and H. J. Choi, Phys. Rev. B **86**, 115435 (2012).
[24] J. Chen, J. Xi, D. Wang, and Z. Shuai, J. Phys. Chem. Lett. **4**, 1443 (2013).
[25] H. Hwang, Y. Kwon, and H. Lee, J. Phys. Chem. C **116**, 20220 (2012).
[26] J. Koo, H. Hwang, B. Huang, H. Lee, H. Lee, M. Park, Y. Kwon, S.-H. Wei, and H. Lee, J. Phys. Chem. C **117**, 11960 (2013).
[27] H. Hwang, J. Koo, M. Park, N. Park, Y. Kwon, and H. Lee, J. Phys. Chem. C **117**, 6919 (2013).
[28] Y. Kwon, H. Shin, and H. Lee, Phys. Rev. B **88**, 201403(R) (2013).
[29] H. Shin, S. Kang, J. Koo, H. Lee, J. Kim, and Y. Kwon, J. Chem. Phys. **140**, 114702 (2014).
[30] W. E. Carlos and M. W. Cole, Surf. Sci. **91**, 339 (1980).
[31] R. A. Aziz, M. J. Slaman, A. Koide, A. R. Allnatt, and W. J. Meath, Mol. Phys. **77**, 321 (1992).
[32] D. M. Ceperley, Rev. Mod. Phys. **67**, 279 (1995).
[33] R. E. Zillich, F. Paesani, Y. Kwon, and K. B. Whaley, J. Chem. Phys. **123**, 114301 (2005).
[34] D. M. Ceperley and B. Bernu, Phys. Rev. Lett. **93**, 155303 (2004).
[35] B. K. Clark and D. M. Ceperley, Phys. Rev. Lett. **96**, 105302 (2006).
[36] M. Boninsegni, A. B. Kuklov, L. Pollet, N. V. Prokof'ev, B. V. Svistunov, and M. Troyer, Phys. Rev. Lett. **97**, 080401 (2006).
[37] A. F. Andreev and I. M. Lifshitz, Sov. Phys. JETP **29**, 1107 (1969).